Double-to-single photoionization ratio of lithium at medium energies

R. Wehlitz,[1,*] M. M. Martinez,[2] J. B. Bluett,[1] D. Lukić,[3] and S. B. Whitfield[4]
[1]*Synchrotron Radiation Center, UW-Madison, Stoughton, Wisconsin 53589, USA*
[2]*University of Washington, Seattle, Washington 98105, USA*
[3]*Institute of Physics, 11001 Belgrade, Serbia and Montenegro*
[4]*Department of Physics and Astronomy, UW–Eau Claire, Eau Claire, Wisconsin 54702, USA*
(Received 4 February 2004; published 14 June 2004)

The double-to-single photoionization ratio of atomic lithium has been measured for photon energies ranging from 120 eV to 910 eV. Through extensive use of various filters we were able to significantly extend the previous range of measurements [M.-T. Huang *et al.*, Phys. Rev. A **59**, 3397 (1999)]. We find that our data are in agreement with the predicted high-energy limit of 3.4%. By applying simple model curves to our data, we believe that sequential processes contribute substantially to the double-photoionization cross-section ratio as predicted by theory.

DOI: 10.1103/PhysRevA.69.062709 PACS number(s): 32.80.Fb

I. INTRODUCTION

Photoionization by a single photon has a well-defined energy and angular momentum transfer (except for Compton scattering) from the photon to the target atom and provides a simple testing ground for theoretical models. Since the photoelectric operator is a one-electron operator, only single-electron excitation or ionization is possible within the framework of the independent-particle model. Therefore, multielectron processes are entirely due to correlation effects among electrons.

Many experiments and theoretical investigations were—and still are—concerned with the double photoionization of He (see, e.g., [1]). From the periodic table, Li represents the next level of sophistication from the He problem because now intershell electron correlation is possible. Also, in contrast to He, there is more than one way to create a doubly charged Li ion. Above the first double-ionization threshold ($1s^{-1}2s^{-1}$) at 81.03 eV [2] double and triple excitations can decay and produce doubly charged ions by—with one exception [3]—emitting two electrons sequentially. As the previous investigation by Huang *et al.* [5] shows, the second double-ionization threshold ($1s^{-2}$) at 172.8 eV [4] is not visible in the double-to-single photoionization ratio. Besides the investigations of the double-to-single photoionization ratio by Huang *et al.* [5] in the energy region from 81 to 424 eV, only two other experimental investigations of this ratio were performed: one of them focused on the $2s^22p$ resonance at 142.33 eV [3], while the other one concentrated on the energy region near the first double-ionization threshold [6,7].

Theoretical investigations of the double-photoionization process in Li are so far limited to the high-energy limit, but calculations at finite photon energies are underway [8]. van der Hart and Greene [9] predict a double-to-single photoionization cross-section ratio at the high-energy limit of 3.37%, similar to the one predicted by Yan [10] of 3.36%. The predicted value of 1.81 by Cooper [11] is clearly lower than the other predicted ratios. van der Hart and Greene also predict a rather large contribution from ca. 40% of sequential processes to the total double-to-single photoionization ratio at the high-energy limit.

In this paper we present measurements of the double-to-single photoionization cross-section ratio from 120 to 910 eV and compare them with a former measurement and theoretical predictions.

II. EXPERIMENT

A. Setup

The experiment was performed at the Aladdin storage ring of the Synchrotron Radiation Center. Monochromatized synchrotron radiation from three different beamlines—namely, the plane grating monochromator (PGM) [12], the Multilayer [13], and the Mark V grasshopper (Mark V) [14] beamlines—were used for the experiment. Because the experiment required in most cases only a moderate energy resolution, the monochromator entrance and exit slits could be opened relatively wide. Only some of the data in the resonance region around 162 eV were taken with a higher resolution on the PGM beamline with entrance and exit slits at 255 μm and 150 μm, respectively, yielding a resolution of 140 meV at 160 eV. The energy resolution of the Multilayer beamline is naturally poor and is about 50 eV at 910 eV, which, however, is still sufficient for this experiment.

The monochromatized photon beam passed through our differential pumping stage which also housed the filter arrays. The capillary in the differential pumping stage is electrically isolated, and the current created by photons striking the capillary can be measured. The chamber was aligned by minimizing this photocurrent which was about 100 pA.

The photon beam intersected the Li vapor emerging from a resistively heated oven. The temperature of the oven was typically 410 °C. The crucible was electrically biased to prevent thermal electrons from reaching the interaction region. The ions created were extracted by a pulsed electrical field across the interaction region, accelerated into a drift tube, and detected by a Z-stack microchannel-plate detector. By

*Electronic address: wehlitz@src.wisc.edu

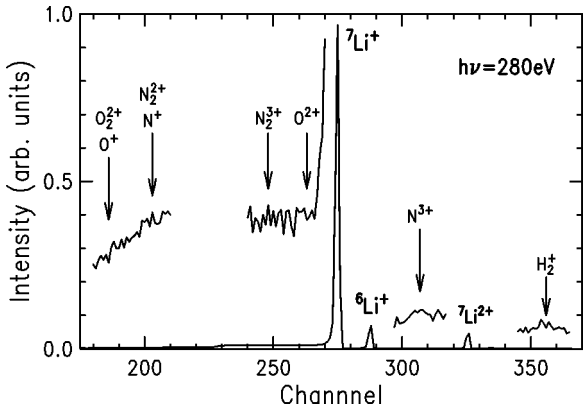

FIG. 1. Li-ion time-of-flight spectrum taken at a photon energy of 280 eV. Note that there is no appreciable amount of residual gas that can affect the area of the Li peaks.

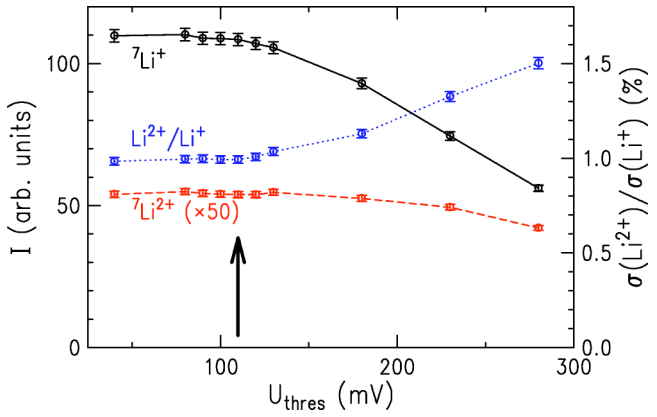

FIG. 2. The relative intensity of the singly and doubly charged Li-ion signal as a function of the CFD threshold U_{thres}. The Li^{2+} intensity is multiplied by 50. The scale for the Li^{2+}:Li^+ ratio is given on the right-hand side. The arrow indicates the threshold voltage used in the experiment.

measuring the ion flight time we obtained a time-of-flight (TOF) ion-yield spectrum [15]. The photon flux was measured with an XUV100 silicon photodiode which has a known quantum efficiency up to 248 eV. Beyond that energy we have applied an extrapolated curve to our photon-flux curves. Knowledge of the absolute photon flux is not necessary for the cross-section ratios.

B. Sample

Li wire packaged in mineral oil was mechanically cleaned with a knife and wiped clean with ethanol. The cleaned wire was transferred into the crucible. The oven was immediately mounted on the chamber and pumped out. The background pressure in the experimental chamber was lower than 1×10^{-8} mbar during the experiment. It is important to have no residual gas, particularly no nitrogen, in the chamber so that no N^{2+} (or N_2^{4+}) overlaps with the Li^+ peak. Figure 1 shows a Li spectrum with no appreciable amount of nitrogen and oxygen. A direct test without Li whether there is a peak at one of the Li-peak positions is inconclusive because the Li sample itself may be the source of nitrogen.

It is worthwhile to mention that the measured isotope ratio ^{6}Li:^{7}Li of 7.4% does not agree with the tabulated value of 8.2%. However, this does not point to an experimental problem, because Li samples are known to have a widespread ^{6}Li abundance "in the range 2.007–7.672 at.%, with natural materials at the higher end of this range" [16] and "commercially available Li materials have atomic weights that range between 6.939 and 6.996…" [16]. A ^{6}Li:^{7}Li ratio of 7.4% yields an atomic weight of 6.95.

C. Experimental parameters

The preamplified (×10) multichannel plate (MCP) pulse was processed by a constant-fraction discriminator (CFD). The threshold of the CFD was set to a sufficiently low level (110 mV) to ensure that there was no difference in the detection efficiency between the singly and doubly charged ions. The threshold was determined experimentally by measuring the Li^+ and Li^{2+} count rates as a function of the CFD threshold as shown in Fig. 2. Since the Li^+ count rate decreases faster than the Li^{2+} count rate with increasing threshold, the Li^{2+}:Li^+ ratio would appear too high if the threshold was at a too high level. Decreasing the threshold more than necessary would result in an increased background in the spectrum.

We also looked at the count rates as a function of the MCP voltage on the front side of the MCP assembly. As is shown in Fig. 3, the count rate rises with increasing MCP voltage but has leveled off around 2700 V for both charge states. While the count rate dependence is slightly different for both charge states, it is the same for both isotopes of Li with the same charge. The count rate for the $^7Li^+$ peak appears slightly smaller for the higher voltages (>2700 V). This can be attributed to the dead time of the electronics because of the very high count rate. For this test we did not use any filter and the $^7Li^+$ signal was unusually strong. We made sure that no dead time occurred during the actual ex-

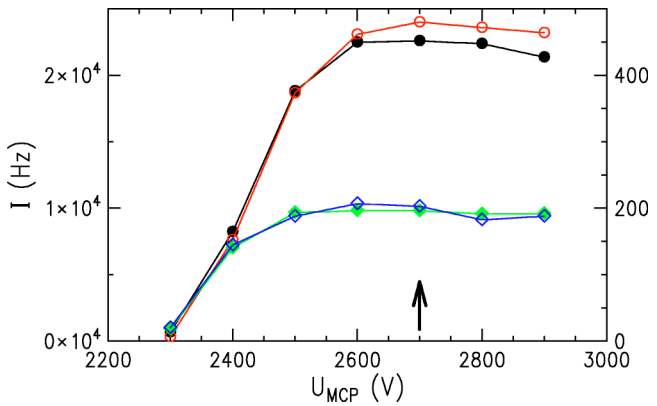

FIG. 3. The count rates for the $^7Li^+$ (solid circles), the $^6Li^+$ (open circles), the $^7Li^{2+}$ (solid diamond), and the $^7Li^{2+}$ (open diamond) peaks as a function of the MCP voltage U_{MCP}. The scale on the left-hand side is for the $^7Li^+$ peak and the scale on the right-hand side is for the $^7Li^{2+}$ peak. The count rates for the ^{6}Li isotope are both divided by 0.074. The arrow indicates the voltage used in the experiment.

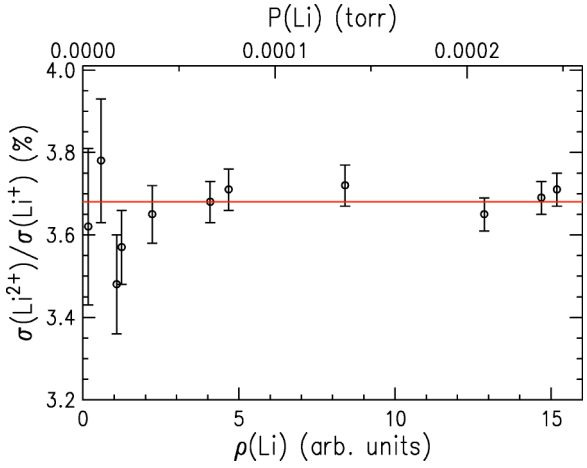

FIG. 4. The double-to-single photoionization cross-section ratio as a function of the Li vapor density ρ and partial vapor pressure P. The horizontal line indicates an average value of the ratio.

periment. Note that the curves for the different isotopes have been scaled to match each other.

It is known from noble gases that the charge-state distribution depends on the gas pressure. Therefore, we have measured the Li^{2+}:Li^{+} ratio as a function of the relative Li vapor density or vapor pressure, which is shown in Fig. 4. The Li vapor density was monitored by the normalized Li^{+} signal as the oven was heated up. From the known oven temperature and using the vapor pressure curves of Honig and Kramer [20], we could approximately relate the density to a partial vapor pressure. Figure 4 does not exhibit any significant pressure dependence in the pressure range shown. This, however, may not be true for even higher vapor pressures. All our data were taken in the pressure range shown in Fig. 4.

D. Filters

Except for the data taken at the PGM undulator beamline, we have employed various filters to suppress nonmonochromatized stray light. Stray light is synchrotron radiation which has scattered off of various beamline components such as the mirrors and grating and has a relatively strong low-photon-energy contribution as the stray light can often be detected by eye. The importance of suppressing stray light has been pointed out in various experimental papers that reported on the double-to-single photoionization ratio of helium; see, e.g., Refs. [17,18]. A good summary of the various possible systematic errors can also be found in Ref. [19].

At the Multilayer beamline we used a 0.3-μm-thick Cu filter. Because the photon energy is set by hand, it was not possible to record a flux curve as a function of photon energy. Therefore, the curve for Cu shown in Fig. 5 is in fact a theoretical transmission curve and is only shown to demonstrate the effectiveness of the Cu filter.

Most of our data were taken at the Mark V beamline where we employed a C filter, Ti filter, and Cr filter of 0.5 μm thickness each. The B filter, installed in the beamline, had an unknown thickness but worked fine as a comparison with our PGM data demonstrates. The corresponding

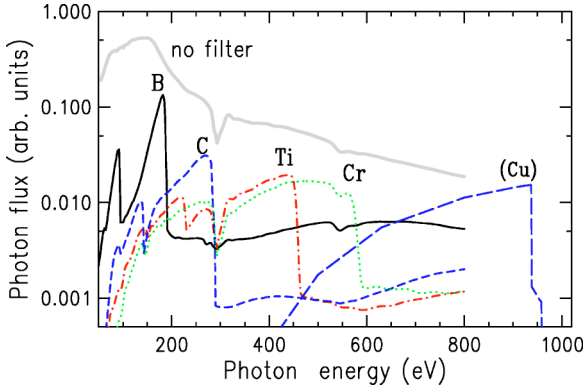

FIG. 5. Photon-flux curves of the Mark V beamline with and without filters. The curve for Cu shows the theoretical transmission of our filter as this filter was used at a different beamline.

flux curves for various filters are shown in Fig. 5. In all flux curves one can see a small dip around 300 eV and 550 eV due to a carbon and oxygen contamination of the beamline mirrors.

Note that the first ionization threshold for Li is at 5.39 eV [2] which makes the Li double-to-single photoionization ratio very susceptible to stray light. While a Pd and Fe filter may work for other elements than Li, they did not work effectively in our case. An insufficient suppression of low-energy stray light results in an artificially increased Li^{+} signal leading to a too low ratio. We noticed that the effectiveness of a filter can be easily checked by monitoring the H_2^{+} peak. Furthermore, we are confident that we have indeed suppressed the stray light, so that its remaining contribution is smaller than our statistical error bars, because we do not see any "kinks" in the ratio when changing from one filter to another.

III. DATA ANALYSIS

In order to determine the photon-energy dependence of the double-to-single photoionization ratio of Li, we took ion time-of-flight spectra at several photon energies using three different beamlines. The areas of the Li^{+} and Li^{2+} ion peaks were numerically integrated. At some photon energies spectra were taken repeatedly and only the average value is shown, which results in a smaller error bar than for points at other energies.

We applied an energy correction to the photon energy, which we determined by taking an ion-yield scan across the Ar $2p_{3/2} \rightarrow 4s$ resonance, which has a well-known energy of 244.39(1)eV [21]. The energy correction was assumed to be a constant shift in wavelength over the energy range of interest. The data taken at the PGM beamline have an energy offset of 0.04 eV but were not corrected because the energy resolution of 0.14 eV is much larger.

IV. RESULTS AND DISCUSSION

A. Overall behavior

Figure 6 shows all our double-to-single photoionization ratios along with the previously published ratios of Huang

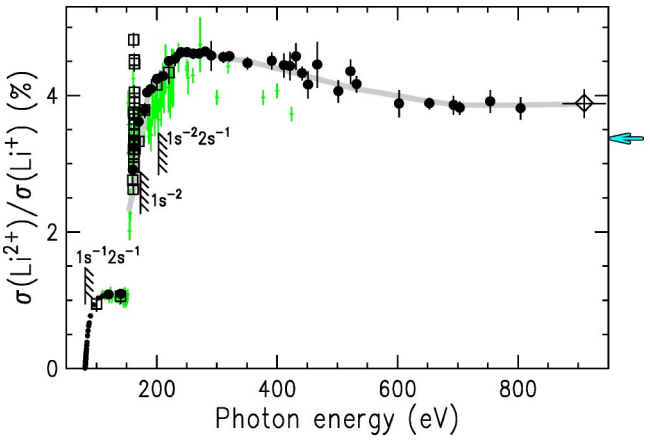

FIG. 6. Double-to-single photoionization cross-section ratio as a function of photon energy: Solid circles: this work (Mark V). Open squares: this work (PGM). Open diamond (at 910 eV): this work (Multilayer). Gray bars: [5]. Small dots below 110 eV: [7]. The arrow marks the theoretical ratio at the high-energy limit [9,10]. The gray curve is a smooth curve through our data points.

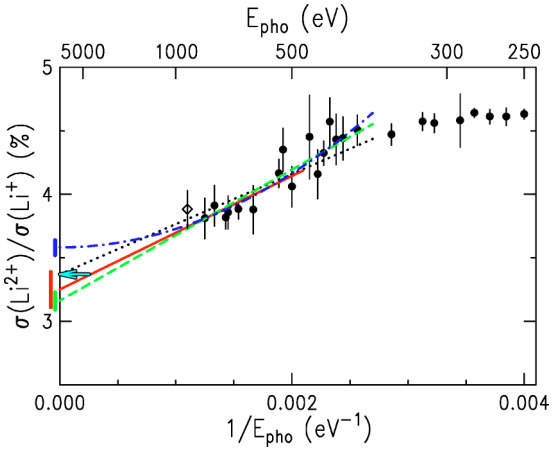

FIG. 8. Same as Fig. 6 but on an inverted photon-energy scale. The solid line and dashed line are linear and the dash-dotted line is a parabolic fit curve to our data. The bars outside the frame are the error bars of the corresponding fit curve. The dotted line is a fit curve starting at the theoretical ratio for the high-energy limit [9,10] which is indicated by an arrow.

et al. [5]. The data of Ref. [5] agree well with our data up to about 240 eV, although they tend to be systematically lower between 190 and 220 eV. Above 250 eV the previous data [5] exhibit a large scattering and are lower than our ratios. The double-to-single photoionization ratio reaches a maximal value of 4.6% at around 250 eV and slowly decreases to 3.9% at 910 eV. Although our spectra were taken with different filters for different energy regions, no obvious kinks in the energy dependence are visible. Also, the ratios taken at different beamlines (represented by different plot symbols in Fig. 6) match very well to each other in their overlapping energy regions.

B. Lower-energy region

The lower-energy region is shown in Fig. 7. Above the first double photoionization (DPI) threshold $1s^{-1}2s^{-1}$

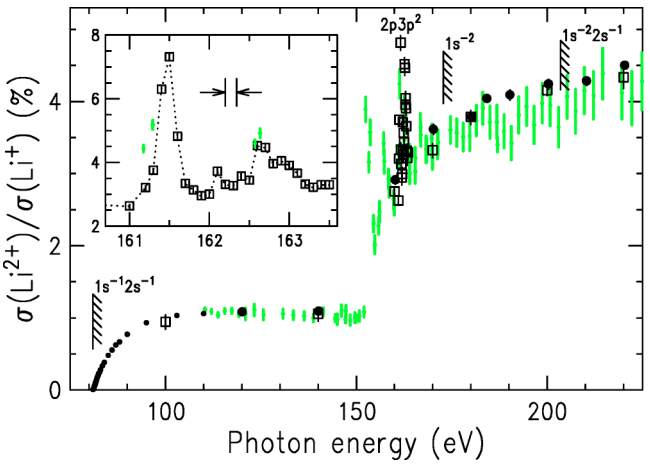

FIG. 7. Same as Fig. 6 but on an enlarged energy scale in the low-energy region. The inset shows the region around the $2p3p^2$ resonance and the arrows indicate the photon-energy resolution. Note that the ordinate of the inset has a different scale.

(81.03 eV) the double-to-single photoionization ratio rises to about 1% and remains essentially flat up to 150 eV where strong double and triple excitations ("hollow lithium" [22,23]) start to increase this ratio significantly. Even at one of the weaker resonances at 161.5 eV—i.e., the *M* resonance according to Ref. [22]—the ratio reaches 7.5% on top of a nonresonant ratio of ca. 3%. Previous measurements [22] show a less enhanced ratio on resonance due to a lower photon-energy resolution as can be seen in the inset of Fig. 7. Since the resonances are rather narrow and require a small photon-energy step size, it would be very time consuming to measure the entire resonance region. Although this is an interesting experiment, our goal was to investigate the ratio at higher photon energies. The following, higher-lying resonances do not show such a strong enhancement anymore. The second DPI threshold $1s^{-2}$ at 172.8 eV does not produce a visible increase of the ratio. Instead, the ratio is continuously climbing up to 4.6% at around 250 eV.

C. High-energy region

Figure 8 shows our Li^{2+}:Li^{+} cross-section ratios on an inverted photon energy scale. This allows us to conveniently extrapolate the ratio to the high-energy limit which appears at 0 eV^{-1} on the inverted energy scale. We made a linear extrapolation for two different energy ranges—namely, for all ratios above 500 eV (solid line) and above 400 eV (dashed line in Fig. 8)—and obtained high-energy limits of 3.16(7)% and 3.25(14)%. Using a parabolic extrapolation of our ratios above 400 eV (dash-dotted line), we obtain 3.58(6)% for the ratio at the high-energy limit. The theoretical predicted values of 3.37% [9] and 3.36% [10] lie within these ratios and are also within the error bar of the extrapolated value of 3.25(14)% obtained by applying a linear extrapolation to our data above 500 eV. Another theoretical value for the high-energy ratio of 1.81% [11] is clearly too low and can be ruled out as the correct high-energy ratio. A

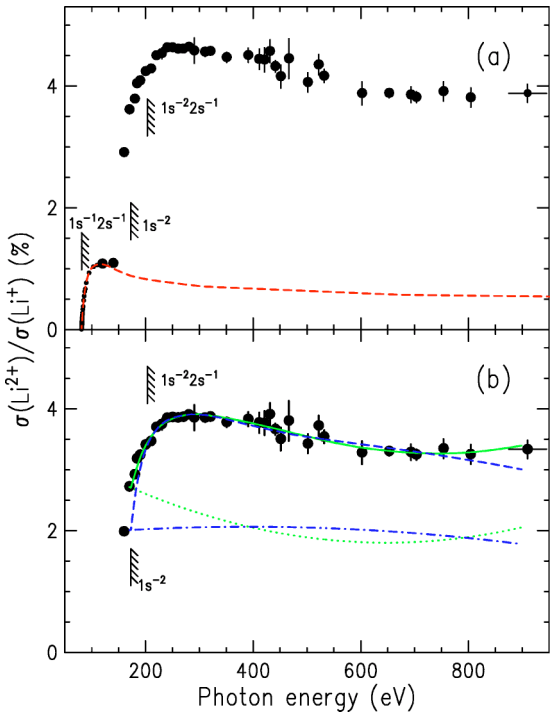

FIG. 9. (a) Same as Fig. 6 but without the data across the resonances shown in the inset of Fig. 7. Dashed line: model curve of the $1s^{-1}2s^{-1}$ double photoionization. (b) Solid circles: ratios of the upper panel reduced by the height of the dashed line in the upper panel. The solid and dashed curves are least-squares fit curves to the data with the dotted and dash-dotted lines as the corresponding background curves. See text for details.

linear "backward" extrapolation from the theoretical ratio of 3.37%—assuming it is correct—towards our data is shown as a dotted line in Fig. 8. Visually, this curve looks just as good as our other fit curves.

D. Modeling of the data

One of the big unanswered questions is how the different processes (simultaneous emission of the 1*s* and 2*s* electrons, simultaneous emission of both 1*s* electrons, and sequential emission of two electrons) contribute to the total double-to-single photoionization ratio. Here, we attempt to shed some light on this problem. We already know that the low-energy part of the $1s^{-1}2s^{-1}$ cross-section ratio, 83–110 eV, can be modeled by the He^{2+}:He^{+} ratio [19] using an appropriate energy scale [7,24]. The double-to-single photoionization ratios of He, Li($1s^{-1}2s^{-1}$), Be($2s^{-2}$), H_2 exhibit the same energy dependence if the energy scale is in units of the energy difference between the particular double- and single-ionization thresholds [24].

Assuming that this energy-scaling model will hold also at higher photon energies, we can tentatively extrapolate the ratio of this process to high photon energies using the He double-to-single photoionization ratio of Samson *et al.* [19]. We have multiplied their He ratio by a factor of 0.289 and the resulting curve is shown as a dashed line in Fig. 9(a) and represents the contribution from simultaneous ejection of a 1*s* and a 2*s* electron. The low-energy part of this curve, where it fits the data, has already been shown in Fig. 4 of Ref. [7].

We now subtract the dashed curve shown in Fig. 9(a) from our data points. The result is shown in panel (b) without the data points taken across the resonances. This ratio is due to the simultaneous ejection of both 1*s* electrons plus the sequential ejection (ionization followed by Auger decay) of two electrons. Note that the data points in the region between the $1s^{-2}$ double ionization threshold (172.8 eV) and the triple-ionization threshold (203.48 eV [2]) may be effected by resonances. Above the triple ionization threshold of Li resonances do not exist anymore. Nevertheless, sequential processes are still possible. For example, one 1*s* electron can be photoionized while the second 1*s* electron gets excited to an np ($n \geqslant 2$) state (satellite), leaving the Li^{+} ion in a $2snp$ state, which then decays, filling the 1*s* hole and ejecting another electron.

The nonradiative decay of satellite lines has been observed previously for Ne and Ar [25,26] and is known to contribute substantially to the total double-photoionization cross section. The satellite-to-1*s* ratio quickly reaches an almost constant value as the photon energy increases, leading to an almost constant contribution of sequential processes to the total double-to-single photoionization ratio. Therefore, we do not expect sudden changes in the contribution from sequential processes to the double-to-single photoionization ratio. In order to test whether our scaling model can be applied to inner-shell double photoionization, we performed a fit in the range from 205 to 900 eV using a properly scaled ratio curve of helium [19] with an additional second-order polynomial curve. This polynomial curve is supposed to approximate the contribution from sequential processes while the helium curve serves as a model for the simultaneous ejection of both 1*s* electrons. The resulting fit curve is shown in Fig. 9(b) as a solid line while the dotted line is the corresponding second-order polynomial. Note that both curves have been extended down to the $1s^{-2}$ threshold.

We also performed a similar fit, but this time with a helium curve that was only shifted to the $1s^{-2}$ threshold but without compressing the energy scale. The resulting fit curve is shown as a dashed line in Fig. 9(b) and the corresponding second-order polynomial is shown as a dash-dotted line.

Both fit curves model our data quite well. Although the first fit curve (solid line) appears to fit our data slightly better in the region below 200 eV, we do not know how much those data points are affected by resonances. Also, the first fit curve seems to be in better agreement with our ratio at 910 eV than the second fit curve. Therefore, at present we can neither confirm nor refute the applicability of our scaling model to the $1s^{-2}$ double-photoionization ratio. Interestingly, however, both second-order polynomial curves which approximate the sequential processes are quite similar at photon energies above 400 eV with a ratio of ca. 1.9% at 900 eV. With a total ratio of 3.88% [see our point at 910 eV in Fig. 9(a)] the contribution from sequential processes seems to be around 50% which is not too far off from a value of "over 40%" predicted by van der Hart and Greene [9] for the high-energy limit. While our analysis does not provide a reliable percentage of the contribution of sequential pro-

cesses to the total double-to-single ionization ratio, it suggests that sequential processes make a substantial contribution to that ratio.

V. CONCLUSIONS

We have determined the double-to-single photoionization cross-section ratio of atomic lithium for photon energies between 120 and 910 eV and have extended previous measurements [5] to higher energies. While the older data are in accord with our new data below 240 eV, the scattering of the older ratios above 240 eV does not appear in our ratios anymore.

The ratio reaches its maximum value of 4.6% around 240 eV and is then slowly decreasing down to 3.9% at 910 eV. We find that our data are in agreement with the predicted [9,10] high-energy limit of 3.4%. We applied simple model curves to our ratios and found that sequential processes contribute substantially to the double-photoionization cross-section ratio consistent with the theoretical prediction of van der Hart and Greene [9].

It is still desirable to have more data at even higher photon energies in order to determine the high-energy limit of the ratio more precisely. Furthermore, we hope that future experiments will be able to separate sequential and simultaneous double-photoionization processes without the need of approximate model curves.

ACKNOWLEDGMENTS

The authors wish to thank the SRC staff for excellent support. Partial financial support by the National Science Foundation (NSF) under Grant No. PHY-9987638 is gratefully acknowledged. One of us (M.M.M.) was supported by the REU program of the National Science Foundation. The SRC is operated under NSF Grant No. DMR-0084402.

[1] J. S. Briggs and V. Schmidt, J. Phys. B **33**, R1 (2000), and references therein.
[2] A. A. Radzig and B. M. Smirnov, *Reference Data on Atoms, Molecules, and Ions* (Springer-Verlag, Berlin, 1985).
[3] R. Wehlitz, M.-T. Huang, K. A. Berrington, S. Nakazaki, and Y. Azuma, Phys. Rev. A **60**, R17 (1999).
[4] C. E. Moore, *Atomic Energy Levels*, Natl. Bur. Stand. (U.S.) Spec. Publ. No. 467 (U.S. GPO, Washington, D.C., 1949), Vol. 1
[5] M.-T. Huang, R. Wehlitz, Y. Azuma, L. Pibida, I. A. Sellin, J. W. Cooper, M. Koide, H. Ishijima, and T. Nagata, Phys. Rev. A **59**, 3397 (1999).
[6] R. Wehlitz, J. B. Bluett, and S. B. Whitfield, Phys. Rev. Lett. **89**, 093002 (2002).
[7] R. Wehlitz, J. B. Bluett, and S. B. Whitfield Phys. Rev. A **66**, 012701 (2002).
[8] J. Colgan and M. S. Pindzola, Bull. Am. Phys. Soc. **48**, 74 (2003).
[9] H. W. van der Hart and C. H. Greene, Phys. Rev. Lett. **81**, 4333 (1998).
[10] Z.-C. Yan, Phys. Rev. A **60**, R3358 (1999).
[11] J. W. Cooper, Phys. Rev. A **59**, 4825 (1999).
[12] R. Reininger, S. L. Crossley, M. A. Lagergren, M. C. Severson, and R. W. C. Hansen, Nucl. Instrum. Methods Phys. Res. A **347**, 304 (1994).
[13] J. F. MacKay, D. W. Pearson, B. E. Nelms, P. M. DeLuca, Jr., and M. N. Gould, Med. Phys. **25**, 773 (1998).
[14] D. J. Wallace, G. C. Rogers, and S. L. Crossley, Nucl. Instrum. Methods Phys. Res. A **347**, 615 (1994).
[15] R. Wehlitz, D. Lukić, C. Koncz, and I. A. Sellin, Rev. Sci. Instrum. **73**, 1671 (2002).
[16] Information regarding the Li isotope composition can be found on the web page of the National Institute of Standards and Technology, http://www.physics.nist.gov/PhysRefData/Compositions/index.html
[17] R. J. Bartlett, P. J. Walsh, Z. X. He, Y. Chung, E.-M. Lee, and J. A. R. Samson, Phys. Rev. A **46**, 5574 (1992).
[18] J. H. McGuire, N. Berrah, R. J. Bartlett, J. A. R. Samson, J. A. Tanis, C. L. Cocke, and A. S. Schlachter, J. Phys. B **28**, 913 (1995).
[19] J. A. R. Samson, W. C. Stolte, Z.-X. He, J. N. Cutler, Y. Lu, and R. J. Bartlett, Phys. Rev. A **57**, 1906 (1998).
[20] R. E. Honig and D. A. Kramer, RCA Rev. **30**, 285 (1969).
[21] G. C. King, M. Tronc, F. H. Read, and R. C. Bradford, J. Phys. B **10**, 2479 (1977).
[22] Y. Azuma, S. Hasegawa, F. Koike, G. Kutluk, T. Nagata, E. Shigemasa, A. Yagishita, and I. A. Sellin, Phys. Rev. Lett. **74**, 3768 (1995).
[23] E. T. Kennedy, Phys. Scr. **T95**, 32 (2001), and references therein.
[24] R. Wehlitz and S. B. Whitfield, J. Phys. B **34**, L719 (2001).
[25] U. Becker, R. Wehlitz, O. Hemmers, B. Langer, and A. Menzel, Phys. Rev. Lett. **63**, 1054 (1989).
[26] U. Becker and R. Wehlitz, Phys. Scr. **T41**, 127 (1992).